Efficient two-step photogeneration of long-lived charges in ground-state charge-transfer complexes of conjugated polymer doped with fullerene

Bakulin, Artem A.; Zapunidy, Sergey A.; Pshenichnikov, Maxim S.; van Loosdrecht, Paul H. M.; Paraschuk, Dmitry Yu.

Published in:
Physical Chemistry Chemical Physics

DOI:
10.1039/b905249f

Publication date:
2009

Efficient two-step photogeneration of long-lived charges in ground-state charge-transfer complexes of conjugated polymer doped with fullerene

Artem A. Bakulin,[a] Sergey A. Zapunidy,[b] Maxim S. Pshenichnikov,*[a] Paul H. M. van Loosdrecht[a] and Dmitry Yu. Paraschuk[b]

Received 16th March 2009, Accepted 7th May 2009
First published as an Advance Article on the web 10th June 2009
DOI: 10.1039/b905249f

Polarization-sensitive time-resolved visible-infrared pump–probe experiments demonstrate that one can efficiently generate long-lived charges in donor–acceptor charge transfer complex (CTC) of conjugated polymer doped with fullerene, MEH-PPV/dinitroanthraquinone/C_{60}. In particular, a strong enhancement of the photoinduced charge generation is observed in the red part of the spectrum, *i.e.* inside the polymer band gap, which makes the current material attractive for photovoltaic applications. The spectroscopic results indicate that enhanced generation of charges is due to a consecutive photoinduced electron transfer from the polymer to the CTC-acceptor in the first step and then, in the second step, to the fullerene. The LUMO energy difference between the CTC-acceptor and fullerene appears to be a key parameter for efficient charge separation in these ternary systems. The results are also discussed in respect to the charge generation processes in widely used polymer–fullerene blends, where formation of weak CTCs has recently been discovered.

1. Introduction

One of the key strategies toward improving the performance of plastic solar cells is the development of low-bandgap polymers allowing more efficient harvesting of the solar light in the red and near-IR spectral regions.[1–3] A complimentary, or possibly alternative, route to low-bandgap organic materials is found in the utilization of Mulliken type[4] donor–acceptor charge-transfer complexes (CTCs) based on conjugated polymers.[5–7] Such CTCs have attracted significant attention as an important intermediate for charge harvesting in widely used photovoltaic polymer–fullerene blends,[8–11] as nonvolatile memory,[12] and as narrow-bandgap electrophotographic materials.[13] The usage of CTCs for photovoltaics has a number of attractive virtues. First, the donor–acceptor interactions result in a CTC absorption band in the optical gap of the polymer. As a consequence, the presence of the CTC enhances the utilization of the low-energy part of the solar spectrum. Second, CTC formation can substantially improve the photooxidation stability of the polymer involved in the CTC,[14] which is of high importance for increasing the life-span of polymer solar cells. Third, the efficiency of charge separation in the polymer CTCs can be close to unity, similar to polymer–fullerene blends.[15] However, the crucial drawback in using polymer-based CTCs in photovoltaic devices is efficient geminate recombination of photogenerated charges.[15–18] This recombination seems to be promoted by high localization of the photogenerated charges in CTCs.

For efficient polymer solar cells, it would be extremely beneficial to combine the aforementioned advantages of conjugated polymer-based CTCs with a long carrier lifetime as provided by polymer–fullerene photovoltaic materials.[19] We have previously suggested[15] that this would become possible if one of the photogenerated charges escapes the parent CTC before recombination occurs (*i.e.* faster than 5 ps). Such an escape route can be realized in a ternary blend of polymer-based CTC with an additional acceptor with higher electron affinity and mobility, *e.g.* fullerene (Fig. 1). In this case, the presence of the CTC-acceptor enhances the photosensitivity in the red and increases the photooxidation stability as a result of the CTC formation with the polymer, while the fullerene accepts the already photogenerated electron and thereby improves the generation of long-lived charges and their collection. As a result, a two-step photoinduced electron transfer occurs: from the polymer to the CTC-acceptor and then to the fullerene.

A similar scenario seems to be involved in the photophysics of the widely used photovoltaic polymer–fullerene blends.

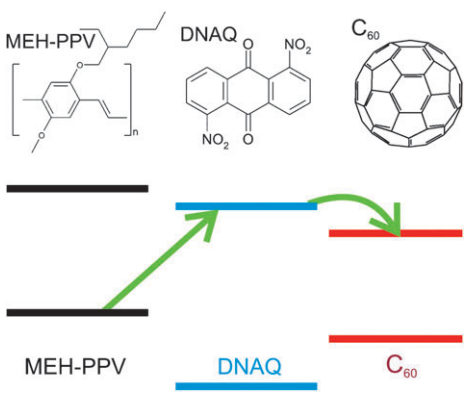

Fig. 1 The chemical structure of materials under study and energies of the frontier molecular orbitals. Arrows show two photoinduced electron-transfer steps.

[a] *Zernike Institute for Advanced Materials, University of Groningen, Nijenborgh 4, 9747 AG Groningen, The Netherlands. E-mail: M.S.Pchenitchnikov@RuG.nl*
[b] *Faculty of Physics and International Laser Center, Lomonosov Moscow State University, Leninskie Gory, 119991 Moscow, Russia*

Although polymer–fullerene CTCs[8,10,16,20–22] are rather weak, making them indiscernible in early studies, their electronic states are an important intermediate on the route from photogenerated excitons to pairs of free charges.[10,20] To reveal the photophysics of CTC-fullerene electron transfer, it would be beneficial to start with an easily observable ground-state CTC as found in blends of the archetypical conjugated polymer MEH-PPV with low-molecular-weight electron acceptors.[6] Such CTCs may serve as a model system providing invaluable insight into the charge generation process in donor-CTC-acceptor systems.

In this paper we demonstrate a proof-of-principle example of the two-step charge separation in the polymer-based CTC doped with fullerene. Ultrafast polarization-sensitive photoinduced absorption spectroscopy (PIA) was used to monitor charge photogeneration and to discriminate consecutive and parallel charge transfer processes. A significant, by a factor of 2, enhancement of the photogeneration efficiency of long-lived charges in the ternary blend compared to the polymer-based CTC was observed. Our results confirm the importance of material lowest unoccupied molecular orbital (LUMO) level management for providing efficient electron harvesting from the CTC states in polymer–fullerene blends.

Experimental details

A conjugated polymer, poly[2-methoxy-5-(2′-ethyl-hexyloxy)-1,4-phenylene vinylene] (MEH-PPV), organic acceptor 1,5-dinitroanthraquinone (DNAQ), and fullerene C_{60}, were chosen as components (Fig. 1) of a model ternary system. One advantage of using this particular blend is that DNAQ is known to form an easily-observable CTC with MEH-PPV with an extended absorption in the red.[6] A second advantage is that according to electrochemical data, the LUMO of C_{60}[23,24] is about 0.4 eV lower than the LUMO of DNAQ[25] (Fig. 1) which favors the charge transfer from CTC to C_{60} in the second step.

For the preparation of binary/ternary blends each component (MEH-PPV, DNAQ, C_{60}) was separately dissolved in chlorobenzene at a concentration of 2 g l^{-1}. Then the solutions were mixed with a weight ratio of components 1 : 0.3 and 1 : 0.2 for binary blends of MEH-PPV/DNAQ and MEH-PPV/C_{60}, respectively, and 1 : 0.3 : 0.2 for the ternary MEH-PPV/DNAQ/C_{60} blend. The donor–acceptor ratio in MEH-PPV/DNAQ blend was chosen as 1 : 0.3 to provide the maximum CTC concentration in the films.[26] Films were prepared by drop-casting on microscope cover-glass substrates. The absorption spectra were recorded with a Perkin-Elmer Lambda 900 spectrophotometer.

Polarization-sensitive time-resolved photoinduced absorption (PIA) experiments were performed with a femtosecond VIS-pump – IR-probe setup described in details elsewhere.[15] Briefly, a home-built Ti : Sapphire multipass amplifier was used to pump a noncollinear optical parametric amplifier[27] providing tunable visible excitation pulses (duration 30 fs, energy 1 μJ per pulse), and an optical parametric amplifier generating the IR probe (70 fs, 0.05 μJ).[28] The probe frequency was positioned at the center of the low-energy (LE) polaron band of MEH-PPV at 0.42 eV.[29] The polarization of the IR probe beam was rotated by 45° with respect to the polarization of the pump beam. After the sample, the probe component parallel or perpendicular to the pump polarization was selected by a wire-grid polarizer (extinction coefficient of 1 : 100) and detected by a liquid-nitrogen-cooled InSb photodiode. The isotropic (population) signal $\Delta T_{iso}(t)$ and the induced anisotropy $r(t)$ were then calculated from the well-known expressions:[30]

$$\Delta T_{iso}(t) = \frac{\Delta T_{||}(t) + 2\Delta T_{\perp}(t)}{3}, \quad (1)$$

$$r(t) = \frac{\Delta T_{||}(t) - \Delta T_{\perp}(t)}{3\Delta T_{iso}(t)}, \quad (2)$$

All PIA transient data were obtained at 300 K in a nitrogen atmosphere.

In the continuous-wave (cw) PIA spectroscopy studies, cw solid-state lasers operating at 532 and 670 nm were employed as a pump source. In the probe channel, we used a tungsten–halogen lamp for illuminating the sample, a monochromator, and solid-state photodetectors (Si and InGaAs). The pump beam was mechanically chopped at 75 Hz, and the PIA signal in the probe channel was processed by a lock-in amplifier at the pump modulation frequency. Photoluminescence of the films was measured using the same set-up.

Results and discussion

The optical absorption and photoluminescence data indicate that addition of C_{60} to the MEH-PPV/DNAQ blend does not affect strongly the CTC formation between MEH-PPV and DNAQ. That is demonstrated in Fig. 2 which compares the normalized absorption spectra of MEH-PPV, MEH-PPV/C_{60}, MEH-PPV/DNAQ, and MEH-PPV/DNAQ/C_{60}. Binary MEH-PPV/DNAQ blend displays a noticeable red shift of the absorption spectrum relative to MEH-PPV, and, more importantly, possesses an enhanced absorption extending deeply into the optical gap of MEH-PPV. These changes were associated with the CTC formation in MEH-PPV/DNAQ

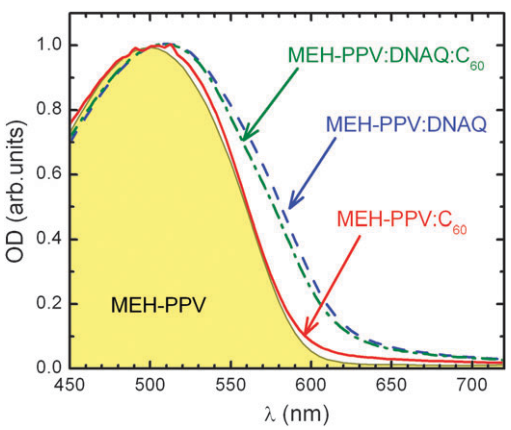

Fig. 2 Normalized absorption spectra of MEH-PPV/C_{60} blend with a weight ratio 1 : 0.2 (solid curve), MEH-PPV/DNAQ 1 : 0.3 (dashed curve), and MEH-PPV/DNAQ/C_{60} 1 : 0.3 : 0.2 (dash-dotted curve) blends. The shaded contour represents the absorption of a MEH-PPV film.

blends.[6,26] Whereas the absorption spectrum of the MEH-PPV/C_{60} blend (solid curve) is a superposition of the individual absorption spectra of MEH-PPV (shaded area) and C_{60} (not shown), the absorption spectrum of MEH-PPV/DNAQ/C_{60} (dash-dot line) blend is quite similar to that of MEH-PPV/DNAQ (dashed line). The slightly less-pronounced red shift of the MEH-PPV absorption edge in the ternary blend can not be explained by a simple superposition of the binary blend absorption spectra. Most probably, it results from a change in the polymer effective conjugation length or/and in the local dielectric environment of the polymer chains in the blend.[26]

In addition to these absorption experiments, we also verified the strong quenching of luminescence which was previously observed in MEH-PPV/DNAQ blends due to efficient exciton dissociation by charge transfer to DNAQ.[6] In the ternary blend, photoluminescence quenching was found to be as efficient as in MEH-PPV/DNAQ CTC, and one order more efficient than in MEH-PPV/C_{60} blend at corresponding acceptor concentrations. This indicates that the exciton dissociation in the ternary blend occurs predominantly due to the CTC formation.

The evolution of photo-induced charges in the polymer was studied by monitoring the transient intensity of the charge-associated absorption band(s) in the photoinduced absorption (PIA) spectra of the blends.[29,31–33] The presence of charge at MEH-PPV leads to the appearance of additional absorption bands in the IR region due to the formation of new allowed states in the polymer bandgap. In particular, the low energy (LE) and high energy (HE) absorption bands at $\sim$3 and $\sim$1 μm, respectively, are the well-known fingerprints of charged states in MEH-PPV.[29] We refer the reader to ref. 15 for the PIA spectra of the blends and a detailed discussion on the advantages of probing the LE band (as is the case in the current study). In our further analysis we assume changes of the LE transition cross-section to be negligibly small so that the charge-associated absorption is proportional to the concentration of charges in the sample.[15]

Fig. 3a shows typical isotropic (*i.e.* polarization independent) PIA transients in the binary and ternary blends. We excited the CTC absorption band with 30-fs pulses centered at 620 nm while monitoring the transient changes at the LE absorption band around $\sim$3 μm. MEH-PPV is almost transparent at the excitation wavelength thereby minimizing its direct photo-excitation and the possible photoinduced electron transfer form MEH-PPV to C_{60}. The PIA transient for the MEH-PPV/DNAQ CTC is characterized by a prominent and fast (<5 ps) multi-exponential decay with a diminutive long-lived component (Table 1). Assuming the PIA amplitude to be proportional to the concentration of polaron states, the PIA decay reflects a decrease in the number of the charges at the MEH-PPV. The observed decay was previously attributed to the fast geminate recombination of photogenerated charges on the basis of photocurrent and transient anisotropy measurements.[15] The (sub)picosecond part of decay can be approximated by two exponents having time constants of 0.7 and 5 ps, with both time scales representing a broad distribution of CTCs in diverse local environments. From fluorescence and transient anisotropy measurements[15,34] the former timescale is known to be characteristic of thermalization in the conjugated

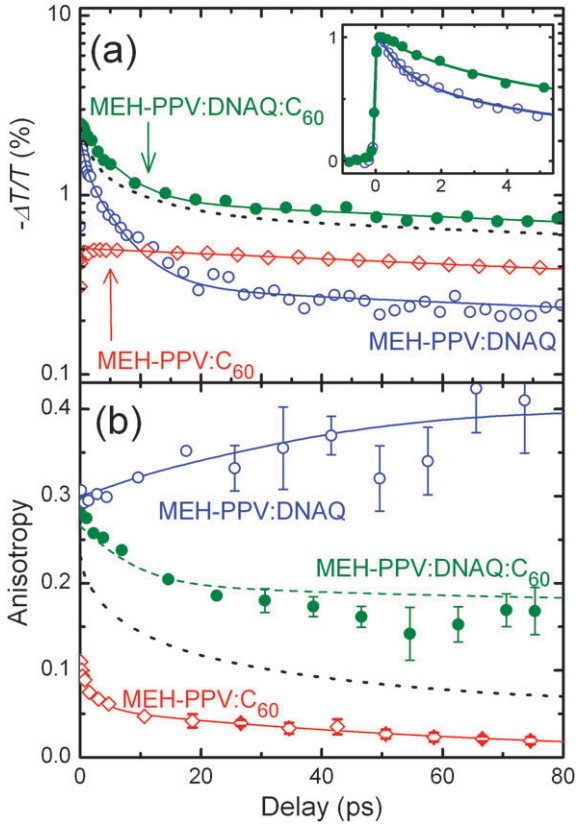

Fig. 3 Isotropic PIA transients (a) and induced anisotropy (b) of the LE band for MEH-PPV/DNAQ (open circles), MEH-PPV/C_{60} blend (diamonds), and MEH-PPV/DNAQ/C_{60} (solid circles) excited at 620 nm. The early part of the isotropic PIA transients is depicted in the inset. Solid curves show multi-exponential fits to the data (for isotropic signals, fit parameters are given in Table 1). Dotted curves display the direct sum of isotropic responses from CTC and MEH-PPV/C_{60} (a), and the anisotropic response as derived from summing up the parallel and orthogonal components of the CTC and MEH-PPV/C_{60} PIA responses and then calculating the anisotropy according to eqn (2) (b). The dashed curve presents the anisotropy calculated according to the model explained in the text.

Table 1 Parameters of the multi-exponential fit $\sum A_i \exp(-t/T_i)$ (i = 1,2,3) of isotropic PIA transients measured after excitation at 620 nm. The sum of amplitudes A_i is normalized to 100%

Material	A_1 (T_1 = 0.7 ps)	A_2 (T_2 = 5.4 ps)	A_3 (T_3 = 0.3 ns)
MEH-PPV/ C_{60}	—	—	100%
MEH-PPV/DNAQ	30%	55%	15%
MEH-PPV/DNAQ/C_{60}	—	60%	40%

polymers. Therefore, we assign sub-ps dynamics to be mostly related to the charge recombination from the "hot" excited states. In the same spirit, we attribute the $\sim$5 ps component to recombination from the already thermalized states. Finally, the minor ($\sim$15%) 0.3 ns component in the decay is attributed to the small fraction of long-lived charges. Previous studies suggested that these charges have low mobility and are probably trapped.[15]

In contrast, PIA kinetics in the MEH-PPV/C_{60} blend can be well approximated by a slow mono-exponential decay with a time constant of $\sim$0.3 ns or longer (Table 1). Therefore, we conclude that there are no changes in the charge concentration during the first 100 ps, indicating that the majority of photogenerated charges are long-lived. The initial (short-time) PIA amplitude in the MEH-PPV/C_{60} blend is low compared to that of the CTC (Fig. 3a) mainly due to the low absorption of MEH-PPV/C_{60} blend at the excitation wavelength. We attribute the observed signal to the excitation of C_{60}.

The PIA transient in the ternary blend MEH-PPV/DNAQ/C_{60} (Fig. 3a, solid circles) is significantly different from that in the MEH-PPV/DNAQ CTC (open circles). Most striking is the disappearance of the fast (0.7 ps) decay upon doping the CTC with C_{60} (Fig. 3a, inset). As a result of this, the amplitude of the long-lived ($>$300 ps) component of the PIA decay becomes higher by a factor of 3 in the ternary blend than in the MEH-PPV/DNAQ CTC (Table 1). This indicates an appreciable increase in the survival probability of the photogenerated charges upon doping with C_{60}. The resulting $\sim$40% yield of the long-lived charges in the ternary blend is comparable with the $\sim$50% yield observed in the widely used MEH-PPV/PCBM blend,[15] and exceeds by a factor of 2 the amount of long-lived charges in the reference MEH-PPV/C_{60} blend (Fig. 3a).

The increase in the efficiency of long-lived charge generation can be attributed to a consecutive electron transfer from the CTC-acceptor to the fullerene within the first ps after excitation. After the charge photogeneration within the CTC and the subsequent (CTC-acceptor)/C_{60} charge transfer, the electron at C_{60} and the hole at MEH-PPV become completely separated. This rapid separation of charges due to two-step electron transfer strongly suppresses geminate recombination. According to our data, only the fast (0.7 ps) decay component is affected by the C_{60} doping (Table 1); the intermediate ($\sim$5 ps) decay does not change much compared to the MEH-PPV/DNAQ CTC. The charge transfer from CTC to C_{60} should therefore be significantly faster than 0.7 ps. The fact that the 5-ps decay component is hardly affected by doping with fullerene suggests that CTC-C_{60} charge transfer is more efficient from the "hot" CTC states. The possible reason for this could be that the binding energy of the charge-transfer exciton is close to the $\sim$0.4 eV energy difference between the LUMOs of DNAQ and C_{60}. Thus, an excess energy required for the efficient charge separation is available only in the "hot" states which are also more susceptible to geminate recombination in the binary blends.

An important issue to address here is whether the charge transfer is consecutive or if there are two independent charge transfer processes—one in the MEH-PPV/DNAQ CTC and one in the MEH-PPV/C_{60} blend—occurring in parallel. If the latter were true, the ternary blend transient should be a simple sum of the respective transients. As shown in Fig. 3a (dotted curve) this simple sum, however, deviates considerably from the ternary blend transient (note the logarithmic scale). While this fact points toward the consecutive nature of the process, it does not provide *per se* enough evidence to discriminate between the two scenarios given the uncertainties in, for instance, signal normalization, sample composition, and film morphology.

A more reliable separation of the contributions from the CTC and fullerene excitations can be achieved in a polarization-sensitive experiment. It has been demonstrated that the orientation of charge-associated transition dipole in conjugated polymers[35] and their CTCs[15] is correlated with the orientation of the initial electronic transition. In contrast, the polymer–fullerene blends show a substantial anisotropy loss within the first 150 fs after excitation. These differences were previously attributed to the stronger spatial localization of photoinduced charges in the CTC as compared to polymer–fullerene blends.[15] Therefore, in the ternary blend, if the charges are generated through the CTC, the initial anisotropy should be as high as in the binary blend with CTC. In contrast, if the charges are generated *via* two parallel processes, the anisotropy in the ternary blend should be an average of the separate anisotropies in the two binary blends weighted with the corresponding isotropic responses. This difference should provide a sufficient contrast to determine the dominant route to the photogenerated charges.

Fig. 3b shows the transient anisotropy in the ternary blend MEH-PPV/DNAQ/C_{60} as well as in the binary MEH-PPV/DNAQ and MEH-PPV/C_{60} blends. Transient anisotropy in the MEH-PPV/DNAQ CTC begins at a value of 0.3 and stays persistently at a high level (the unusual increase of the anisotropy with time was explained in ref. 15 and is not relevant to the current discussion). In contrast, the anisotropy in MEH-PPV/C_{60} is substantially reduced (to a value of $\sim$0.1) already in the first 100 fs after excitation, and rapidly decays further. The initial anisotropy in the MEH-PPV/DNAQ/C_{60} ternary blend is 0.28 which is close to the 0.3 value observed in the MEH-PPV/DNAQ blend, and exceeds the initial anisotropy in the MEH-PPV/C_{60} blend by a factor of 3. Furthermore, the measured anisotropy dynamics are totally different from those calculated on the basis of the two binary blend responses (dotted curve in Fig. 3b). Note that the anisotropy is not an additive quantity (consult eqn (2)), and, therefore, the (weighed) sum of the two respected anisotropies does not provide the right answer. Instead, parallel (orthogonal) polarization PIA responses of the two binary blends should be summed up, and from the resulted transients the expected anisotropy is calculated according to eqn (2). The dissimilarity between the experimentally measured and calculated anisotropies presents a strong evidence that the generation of long-lived charges in the ternary blend corresponds to the consecutive electron transfer from MEH-PPV to DNAQ and then to C_{60}.

To describe the observed anisotropy dynamics, we build up a model of ultrafast charge dynamics in the ternary blend (Fig. 4) based on the following observations. First, the overall survival probability of long-lived charges in the ternary blend was measured to be $\sim$40% (Fig. 3a, Table 1). Second, based on the PIA experiments on the binary blend, we consider all the charges generated through MEH-PPV/C_{60} excitation to be long-lived (Table 1). Third, the initial anisotropy value of 0.28 in the ternary blend implies that $\sim$85% of the initially excited charges originate from CTC excitation, while the rest (*i.e.* $\sim$15%) appears due to the residual MEH-PPV/C_{60} excitation (Fig. 3b). This is also consistent with the absorption spectra of MEH-PPV/C_{60} and MEH-PPV/DNAQ/C_{60} (Fig. 2)

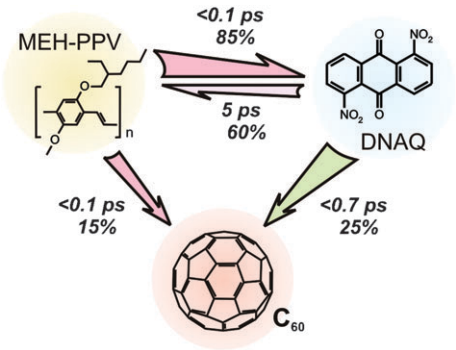

Fig. 4 Schematic representation of the kinetic model summarizing the results of ultrafast PIA experiments in the ternary blend photoexcited at 620 nm. Arrows indicate the charge-transfer pathways. Percentages are calculated with respect to amount of the initially excited charges.

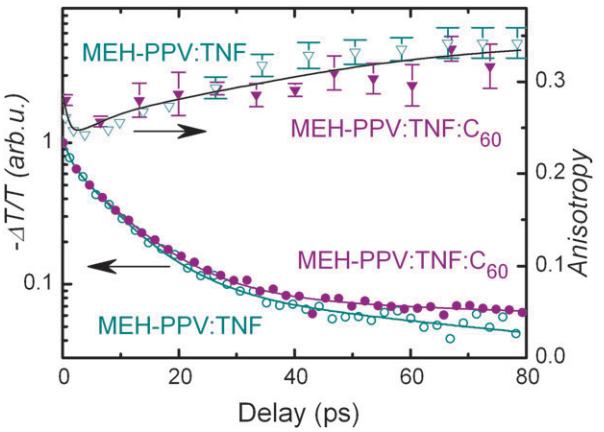

Fig. 5 Isotropic PIA transients (circles) and transient anisotropy (triangles) of the LE band for binary MEH-PPV/TNF (open symbols) and ternary MEH-PPV/TNF/C_{60} (solid symbols) blends, excited at 620 nm. Solid curves show multi-exponential fits to isotropic transients and guide to the eye for anisotropic transient.

and the relative amplitudes of isotropic PIA transients at 0 fs delay (Fig. 3a). Finally, we assume the anisotropy of the charges generated through the CTC to be constant and equal to 0.3.[15] Within this model, the transient anisotropy in the ternary blend can be well reproduced (Fig. 3b, dashed curve) when assuming 25% of initially generated charges to be irreversibly transferred from DNAQ to C_{60} (Fig. 4). The partial anisotropy decay in the ternary blend results from a simple interplay between the short-lived component with high anisotropy (60% of initially generated charges recombine in the CTC) and the long-lived component with low anisotropy provided by MEH-PPV/C_{60} excitation (about 15% of initially generated charges). The ps anisotropy decay in the ternary blend is similar to the one in MEH-PPV/C_{60} blend which was previously assigned to the fast charge transport through the polymer.[15,35]

Efficient photoinduced charge separation in a MEH-PPV/DNAQ CTC doped by fullerene agrees with the fact that the fullerene LUMO is lower in energy than the CTC-acceptor LUMO. To investigate the role of the acceptor electron affinity in the photophysics of the ternary blends, we performed similar experiments with another acceptor, 2,4,7-trinitrofluorenone (TNF), which is also known to form a ground-state CTC with MEH-PPV.[6] The LUMO of TNF[36] is situated at about the same energy as the LUMO of C_{60} [24] thereby making the sequential charge transfer from CTC to C_{60} less probable. Indeed, isotropic PIA transients for the MEH-PPV/TNF/C_{60} ternary blend are almost identical to those for the binary MEH-PPV/TNF blend (Fig. 5) indicating no surplus of the long-lived charges. Also, the anisotropy transients for binary and ternary blends are hardly distinguishable. Therefore, both experiments demonstrate an extremely low efficiency of charge transfer from the CTC to the fullerene resulting from the small (if any) downhill difference in the LUMO energies between TNF and C_{60}.

We have also performed similar PIA and anisotropy experiments in the ternary blends upon excitation in the polymer absorption band (at 540 nm) with the results quite similar to those outlined above (*i.e.* after the CTC band excitation). This, on the one hand, supports our previous conclusion that CTC dominates the photophysics of the material. On the other hand, it confirms the consecutive charge-transfer scenario because similar photophysics for such different excitation wavelengths can not be explained as a superposition of two parallel (MEH-PPV/DNAQ and MEH-PPV/C_{60}) processes.

The ultrafast PIA studies have addressed the early dynamics of photoinduced charges. However, the behavior of the separated charges at longer timescales could be substantially different. The long-time survivability of charges up to the millisecond scale (provided by a mechanical chopper) can be verified by performing PIA experiments under continuous-wave photoexcitation.[31] In our experiments, both the HE band ($\sim$1.3 eV) and the high-energy tail of the LE band ($\sim$0.8 eV) were used as a probe for the photoinduced charges (Fig. 6). These bands are clearly visible in the PIA spectrum of the MEH-PPV/C_{60} blend upon 532 nm excitation, *i.e.* where the polymer is highly absorptive (orange solid curve). Photoexcitation of the binary MEH-PPV/C_{60} blend at 670 nm (that is, at the polymer bandgap) does not result in any PIA signal within experimental accuracy because blend absorption is too low (Fig. 2).[37] Photoexcitation of the binary MEH-PPV/DNAQ blend at 670 nm which matches the tail of the CTC absorption band (Fig. 6, blue dashed curve) does not lead to efficient generation of the long-lived charges, due to their ultrafast and efficient recombination. However, addition of C_{60} to the MEH-PPV/DNAQ blend results in a $\sim$20-fold increase in the PIA intensity of the HE band (Fig. 6, green curve). Furthermore, the PIA signals from the ternary blend MEH-PPV/DNAQ/C_{60} excited in the CTC band and in the binary MEH-PPV/C_{60} blend excited in the polymer absorption band have similar amplitudes after normalization by the number of photons absorbed in the samples. Therefore, after the CTC photoexcitation, the C_{60} facilitates generation of photoinduced charges even at long (up to 10 ms) time scales. The efficiency of charge generation in the ternary blend is close to that in the MEH-PPV/C_{60} blend. However, the higher absorption of ternary blends in the red does provide a dramatic enhancement in the amount of photogenerated charges. In accordance with the time-resolved data, we did

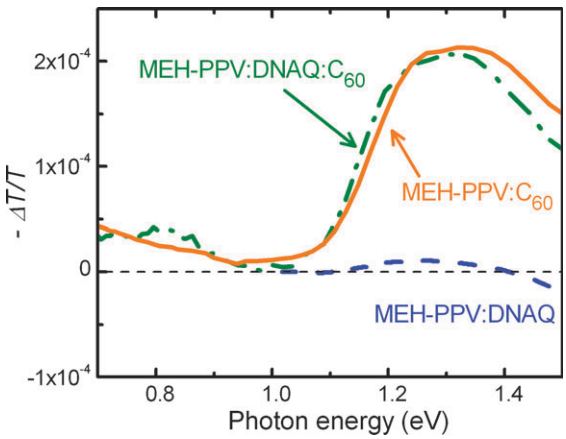

Fig. 6 PIA spectra of 1 : 0.3 : 0.15 MEH-PPV/DNAQ/C_{60} (dash-dot) and 1 : 0.3 MEH-PPV/DNAQ (dashed) blends under cw photoexcitation at 670 nm. The solid curve represents the PIA spectrum in the MEH-PPV/C_{60} blend excited at 532 nm. The absorbed pump-photon fluxes were identical for all measurements.

not observe any enhancement in the cw PIA spectra upon doping the MEH-PPV/TNF CTC by C_{60}.

Our study demonstrates that the CTC excited state can be an efficient intermediate in charge separation if the energy difference between CTC and acceptor LUMO levels is about 0.4 eV (*i.e.* like in MEH-PPV/DNAQ/C_{60}). In contrast, if the energy difference between LUMO levels of CTC-acceptor and detached acceptor is much smaller (*i.e.* like in MEH-PPV/TNF/C_{60}), the second charge separation step is not efficient enough to suppress recombination. The latter mimics the case of the binary phase-separated donor–acceptor blends where only minor interfacial fractions of donor and acceptor form CTCs and, thus, the CTC-acceptor and detached acceptor are the same type of molecules.[10,11,18,22] Indeed, it was previously shown that in such blends the recombination efficiency strongly depends on the donor–acceptor ratio, which determines the density of the interface states[21] assigned to the CTC.[8,10,20] Importantly, the recombination can be overcome by blend annealing[21] that may change the alignment of the relevant LUMO energy levels and create an energy gradient for further charge separation.

Conclusions

With optical time-resolved and cw pump–probe techniques, we have demonstrated that doping of conjugated polymer CTCs with fullerene C_{60} results in a strong enhancement of the photogeneration efficiency of long-lived charges. Their amount in the ternary MEH-PPV/DNAQ/C_{60} blend under red excitation is at least a factor of two higher than in the reference MEH-PPV/C_{60} binary blend. The time-resolved polarization-sensitive data strongly suggest that the generation of such charges corresponds to the consecutive electron transfer from the polymer to the acceptor involved in CTC, and then to the stronger fullerene acceptor. Our proof-of-principle study highlights a promising route to low-bandgap photovoltaic materials based on ternary polymer/(CTC acceptor)/fullerene blends. The discussed approach allows combining the benefits of conjugated polymer CTCs such as strong absorption in the polymer optical gap and enhanced photooxidation stability with the advantages of fullerenes such as efficient agents in generation of charge-separated states and high charge mobility. Preliminary experiments on photovoltaic-device prototypes have indicated a noticeable (up to 30%) increase of the external quantum efficiency of the ternary-blend cells as compared to MEH-PPV/C_{60} in the red part of the spectrum. Further evaluation of the charge collection efficiency in the ternary blends materials is underway.

Acknowledgements

We thank J. Krylova for photoluminescence measurements, V. Dyakonov and D. Martyanov for fruitful discussions, M. Donker and D. Fishman for experimental assistance, and B. Hesp for proofreading the manuscript. This study was in part financially supported by the Russian Foundation for Basic Research (project 08-02-12170-ofi).

References

1 C. J. Brabec, C. Winder, N. S. Sariciftci, J. C. Hummelen, A. Dhanabalan, P. A. van Hal and R. A. J. Janssen, *Adv. Funct. Mater.*, 2002, **12**, 709.
2 M. C. Scharber, D. Mühlbacher, M. Koppe, P. Denk, C. Waldauf, A. J. Heeger and C. J. Brabec, *Adv. Mater.*, 2006, **18**(6), 789.
3 J. Y. Kim, K. Lee, N. E. Coates, D. Moses, T.-Q. Nguyen, M. Dante and A. J. Heeger, *Science*, 2007, **317**, 222–225.
4 R. S. Mulliken, *J. Am. Chem. Soc.*, 1950, **72**, 600.
5 P. J. Skabara, I. M. Serebryakov, I. F. Perepichka, N. S. Sariciftci, H. Neugebauer and A. Cravino, *Macromolecules*, 2001, **34**, 2232.
6 A. A. Bakulin, S. G. Elizarov, A. N. Khodarev, D. S. Martyanov, I. V. Golovnin, D. Yu. Paraschuk, M. M. Triebel, I. V. Tolstov, E. L. Frankevich, S. A. Arnautov and E. M. Nechvolodova, *Synth. Met.*, 2004, **147**, 221–225.
7 P. Panda, D. Veldman, J. Sweelssen, J. J. A. M. Bastiaansen, B. M. W. Langeveld-Voss and S. C. J. Meskers, *J. Phys. Chem. B*, 2007, **111**, 5076–5081.
8 J. J. Benson-Smith, L. Goris, K. Vandewal, K. Haenen, J. V. Manca, D. Vanderzande, D. D. C. Bradley and J. Nelson, *Adv. Funct. Mater.*, 2007, **17**, 451–457.
9 T. Drori, C.-X. Sheng, A. Ndobe, S. Singh, J. Holt and Z. V. Vardeny, *Phys. Rev. Lett.*, 2008, **101**(3), 037401.
10 K. Vandewal, A. Gadisa, W. D. Oosterbaan, S. Bertho, F. Banishoeib, I. V. Severen, L. Lutsen, T. J. Cleij, D. Vanderzande and J. V. Manca, *Adv. Funct. Mater.*, 2008, **18**, 2064–2070.
11 Z. Xu and B. Hu, *Adv. Funct. Mater.*, 2008, **18**, 2611–2617.
12 J.-S. Choi, J.-H. Kim, S.-H. Kim and D. H. Suh, *Appl. Phys. Lett.*, 2006, **89**, 152111.
13 I. F. Perepichka, A. F. Popov, T. V. Orekhova, M. R. Bryce, A. M. Andrievskii, A. S. Batsanov, J. A. K. Howard and N. I. Sokolov, *J. Org. Chem.*, 2000, **65**, 3053.
14 I. V. Golovnin, A. A. Bakulin, S. A. Zapunidy, E. M. Nechvolodova and D. Yu. Paraschuk, *Appl. Phys. Lett.*, 2008, **92**, 243311.
15 A. A. Bakulin, D. S. Martyanov, D. Yu. Paraschuk, M. S. Pshenichnikov and P. H. M. van Loosdrecht, *J. Phys. Chem. B*, 2008, **112**, 13730.
16 L. Goris, K. Haenen, M. Nesladek, P. Wagner, D. Vanderzande, L. d. Schepper, J. D'Haen, L. Lutsen and J. V. Manca, *J. Mater. Sci.*, 2005, **40**, 1413–1418.
17 D. Veldman, O. Ipek, S. C. J. Meskers, J. Sweelssen, M. M. Koetse, S. C. Veenstra, J. M. Kroon, S. S. v. Bavel, J. Loos and R. A. J. Janssen, *J. Am. Chem. Soc.*, 2008, **130**, 7721.
18 I.-W. Hwang, D. Moses and A. J. Heeger, *J. Phys. Chem. C*, 2008, **112**, 4350–4354.

19 N. S. Sariciftci, L. Smivowits, A. J. Heeger and F. Wuld, *Science*, 1992, **258**, 1474.
20 M. Hallermann, S. Haneder and E. D. Como, *Appl. Phys. Lett.*, 2008, **93**, 053307.
21 I.-W. Hwang, C. Soci, D. Moses, Z. Zhu, D. Waller, R. Gaudiana, C. J. Brabec and A. J. Heeger, *Adv. Mater.*, 2007, **19**, 2307–2312.
22 H. Ohkita, S. Cook, Y. Astuti, W. Duffy, S. Tierney, W. Zhang, M. Heeney, I. McCulloch, J. Nelson, D. D. C. Bradley and J. R. Durrant, *J. Am. Chem. Soc.*, 2008, **130**, 3030–3042.
23 D. Dubois, G. Moninot, W. Kutner, M. T. Jones and K. M. Kadish, *J. Phys. Chem.*, 1992, **96**(7137).
24 C. A. Reed and R. D. Bolskar, *Chem. Rev.*, 2000, **100**, 1075.
25 T. Yamamoto, Y. Muramatsu, B. L. Lee, H. Kokubo, S. Sasaki, M. Hasegawa, T. Yagi and K. Kubota, *Chem. Mater.*, 2003, **15**, 4384.
26 V. V. Bruevich, T. S. Makhmutov, S. G. Elizarov, E. M. Nechvolodova and D. Yu. Paraschuk, *J. Chem. Phys.*, 2007, **127**, 104905.
27 G. Cerullo, M. Nisoli, S. Stagira and S. D. Silvestri, *Opt. Lett.*, 1998, **23**(16), 1283.
28 S. Yeremenko, A. Baltuska, F. de Haan, M. S. Pshenichnikov and D. A. Wiersma, *Opt. Lett.*, 2002, **27**, 1171.
29 X. Wei, Z. V. Vardeny, N. S. Sariciftci and A. J. Heeger, *Phys. Rev. B: Condens. Matter Mater. Phys.*, 1996, **53**(5), 2187.
30 R. G. Gordon, *J. Chem. Phys.*, 1966, **45**(5), 1643.
31 N. S. Sariciftci, L. Smivowits, R. Wu, C. Gettinger, A. J. Heeger and F. Wuld, *Phys. Rev. B: Condens. Matter Mater. Phys.*, 1992, **47**(20), 13835.
32 D. Moses, A. Dogariu and A. J. Heeger, *Chem. Phys. Lett.*, 2000, **316**, 356–360.
33 V. Gulbinas, Y. Zaushitsyn, V. Sundström, D. Hertel, H. Bässler and A. Yartsev, *Phys. Rev. Lett.*, 2002, **89**, 107401.
34 S. Westenhoff, W. J. D. Beenken, R. H. Friend, N. C. Greenham, A. Yartsev and V. Sundstrom, *Phys. Rev. Lett.*, 2006, **97**, 166804.
35 J. G. Müller, J. M. Lupton, J. Feldmann, U. Lemmer, M. C. Scharber, N. S. Sariciftci, C. J. Brabec and U. Scherf, *Phys. Rev. B: Condens. Matter Mater. Phys.*, 2005, **72**, 195208.
36 J. E. Kuder, J. M. Pochan, S. R. Turner and D. F. Hinman, *J. Electrochem. Soc.*, 1978, **125**, 1750.
37 In contrast to Vardeny and co-workers[9] we did not observe any polaron response in the MEH-PPV/C60 blend after red excitation, most probably because of lower sample OD (4 *vs.* 1 in our case) and higher sample temperature (70 K *vs.* 300 K, respectively).

